Nanoindentation and wear properties of Ti and Ti-TiB composite materials produced by selective laser melting

H. Attar, S. Ehtemam-Haghighi, D. Kent, I.V. Okulov, H. Wendrock, M. Bönisch, A.S. Volegov, M. Calin, J. Eckert, M.S. Dargusch

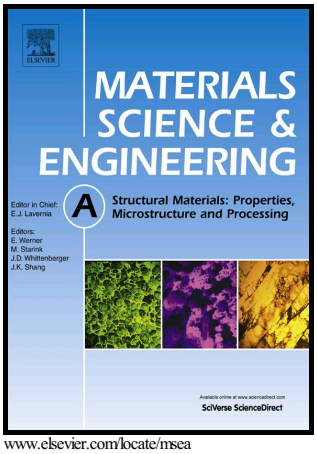

www.elsevier.com/locate/msea

PII: S0921-5093(17)30132-6
DOI: http://dx.doi.org/10.1016/j.msea.2017.01.096
Reference: MSA34658

To appear in: *Materials Science & Engineering A*

Received date: 6 December 2016
Revised date: 25 January 2017
Accepted date: 27 January 2017

Cite this article as: H. Attar, S. Ehtemam-Haghighi, D. Kent, I.V. Okulov, H. Wendrock, M. Bönisch, A.S. Volegov, M. Calin, J. Eckert and M.S. Dargusch, Nanoindentation and wear properties of Ti and Ti-TiB composite materials produced by selective laser melting, *Materials Science & Engineering A* http://dx.doi.org/10.1016/j.msea.2017.01.096

Nanoindentation and wear properties of Ti and Ti-TiB composite materials produced by selective laser melting

H. Attar [a *], S. Ehtemam-Haghighi [b], D. Kent [a, c], I.V. Okulov [d], H. Wendrock [e], M. Bö nisch [e], A.S. Volegov [f], M. Calin [e], J. Eckert [g, h], M. S. Dargusch [a]

[a] *Queensland Centre for Advanced Materials Processing and Manufacturing, School of Mechanical and Mining Engineering, The University of Queensland, Brisbane, Queensland 4072, Australia*

[b] *School of Engineering, Edith Cowan University, 270 Joondalup Drive, Joondalup, Perth, WA 6027, Australia*

[c] *School of Science and Engineering, University of the Sunshine Coast, Maroochydore DC, QLD 4558, Australia*

[d] *Helmholtz-Zentrum Geesthacht, Institute of Materials Research, Division of Materials Mechanics, Geesthacht, Germany*

[e] *IFW Dresden, Institute for Complex Materials, P.O. Box 270116, D-01171 Dresden, Germany*

[f] *Ural Federal University, Institute of Natural Sciences and Mathematics, 620002 Yekaterinburg, Russia*

[g] *Erich Schmid Institute of Materials Science, Austrian Academy of Sciences, Jahnstraße 12, A-8700 Leoben, Austria*

[h] *Department Materials Physics, Montanuniversität Leoben, Jahnstraße 12, A-8700 Leoben, Austria*

E-mails: h.attar@uq.edu.au,

hooyar.attar@gmail.com

[*]Corresponding author (H. Attar):

Abstract:

Ti and Ti-TiB composite materials were produced by selective laser melting (SLM). Ti showed an α′ microstructure, whereas the Ti-TiB composite revealed a distribution of needle-like TiB particles across an α-Ti matrix. Hardness (H) and reduced elastic modulus (E_r) were investigated by nanoindentation using loads of 2, 5 and 10 mN. The results showed higher H and E_r values for the Ti-TiB than Ti due to the hardening and stiffening effects of the TiB reinforcements. On increasing the nanoindentation load, H and E_r were decreased. Comparison of the

nanoindentation results with those derived from conventional hardness and compression tests indicated that 5 mN is the most suitable nanoindentation load to assess the elastic modulus and hardness properties. The wear resistance of the samples was related to their corresponding H/E_r and H^3/E_r^2 ratios obtained by nanoindentation. These investigations showed that there is a high degree of consistency between the characterization using nanoindentation and the wear evaluation from conventional wear tests.

Keywords: Selective laser melting; Nanoindentation; Titanium material; Mechanical property; Wear

1. Introduction

Titanium materials possess good mechanical properties, excellent corrosion resistance and high biocompatibility which make them outstanding candidates for various applications in the biomedical, aerospace and automotive industries [1-4]. Over the past years, a large number of titanium materials have been developed especially in the biomedical area [5-10]. Among them, commercially pure titanium (CP-Ti) is still one of the most commonly used metallic biomaterial for implants [1]. Due to their enhanced properties Ti-TiB composites have the potential to be used not only for biomedical applications, but also in the aerospace and automotive industries in particular due to their improved wear and strength properties [11, 12].

Nowadays, fabrication of complex-shape titanium parts with desirable properties is in high demand. In recent years, selective laser melting (SLM), a 3D metal printing technology, has received a great deal of attention for processing various metallic parts from aluminium [13], Inconel [14], steel [15] and even bronze materials [16]. Various types of titanium materials have been also developed using SLM [17-20], since this technology is not only able to produce complex-shape parts in a highly efficient way, but it also possesses great potential to provide

properties comparable or even superior to those produced by other common commercial methods [21, 22]. The SLM technology has been demonstrated to be highly compatible with processing of titanium materials, representing another key advantage of this technology [23].

In general, the rapid melting and cooling rates associated with the condensed laser source applied during SLM processing can influence microstructure and, consequently, the resulting mechanical and wear properties of SLM-processed materials. Therefore, it is important to study the properties of SLM-processed materials and their relationship to processing variables involved in order to ensure that they can meet demanding performance requirements. Although conventional testing methods are widely used for measuring the mechanical properties of materials, these techniques often require bulk, standard sample geometries which can make them unsuitable for testing samples with specific attributes such as small sample sizes or irregular shapes and geometries. Nanoindentation is a well-established method for measuring the mechanical properties of a wide range of materials especially when a non-destructive approach is required [24, 25]. The advantage of using nanoindentation techniques in comparison to conventional testing methods includes the ability for in-situ measurement of material properties without disrupting the microstructure and causing significant damage. Additionally, no special conditions are required regarding the size and shape of the test samples.

To our best knowledge, nanoindentation investigations of SLM-processed titanium materials with a comparative assessment to conventional mechanical and wear tests have not been carried out. Previous investigations [26] have shown that 3D metal printing of titanium matrix composites with improved wear properties are necessary to broaden the scope of applications for titanium materials, particularly for those involving wear and friction. Therefore, this work evaluates the nanoindentation properties (hardness and elastic modulus) of CP-Ti and Ti-TiB materials produced by SLM. It compares the resulting properties with those derived from conventional mechanical tests. In addition, the study evaluates the wear properties of CP-Ti and Ti-TiB

composite and the fundamental wear mechanisms involved. The work provides a guide to suitable nanoindentation loads for assessing the mechanical and wear properties of SLM-produced CP-Ti and Ti-TiB composite materials.

2. Experimental

Commercially pure titanium (CP-Ti) powder and a blended mixture of Ti-5 wt.% TiB_2 powders were applied for SLM processing using an SLM Solutions machine (MTT SLM 250 HL) under the protection of argon gas. SLM is a bed process in which a powerful laser beam selectively scans across a powder bed, thus selectively melting the exposed powders, which solidify to make a solid layer. Afterwards, a new powder layer is deposited on top of the previously formed solid layer and the cycle continues until the fabrication of component is complete [27]. A set of laser processing parameters including energy density of 120 J/mm^3 combined with a zigzag manufacturing pattern were applied in order to produce almost fully dense samples. The density of the SLM-produced samples was measured using Archimedes' principle. The relative density of the samples was measured to be more than 99.7%.

Prior to performing microstructural, nanoindentation and wear studies, samples were sectioned by a Struers cutting device. Their surfaces were then mechanically ground followed by polishing using standard metallographic procedures. Samples were also etched for microstructural characterizations and were examined using a Zeiss Gemini scanning electron microscope (SEM) and a Tecnai T20 transmission electron microscope (TEM) operated at 200 kV. Samples for TEM investigation were prepared by cutting thin lamellae with Ga ions using the focused ion beam (FIB) technique. A CP-Ti specimen fabricated by casting was also used for comparison between the microstructures obtained from SLM to those from casting.

The mechanical properties of the SLM-produced samples were investigated using nanoindentation. The dimensions of the disk samples used for nanoindentation were 5 mm in diameter and 3 mm in thickness. A Fused Silica reference sample was used for calibration before

conducting the nanoindentation tests. The nanoindentation tests were performed on the SLM-produced samples using a UNAT SEM 2 from ASMEC equipped with a Berkovich pyramidal-shaped indenter tip. Three different loads of 2, 5 and 10 mN with a constant loading rate of 20 μN/s were applied on the polished surface of the samples and at least 50 indentations per load were made. In general, elastic modulus and hardness are measured using Oliver-Pharr analysis [28] or continuous stiffness measurement (CSM) technique [29]. In the current work, Oliver-Pharr analysis [28] was used to determine hardness and reduced elastic modulus of the samples with the reduced elastic modulus (E_r) calculated from the unloading curves.

Generally, the hardness (H) is defined as the ratio of the maximum load (P_{max}) to the projected area of the indentation (A_c) according to the following equations [30]:

$$H = \frac{P_{max}}{A_c} \quad (1)$$

$$A_c = f\left({h_c}^2\right) = 24.5{h_c}^2 \quad (2)$$

where h_c is the contact depth at the peak load and can be calculated based on the equation below [30]:

$$h_c = h_{max} - \varepsilon\frac{P_{max}}{S} \quad (3)$$

where h_{max} is the displacement at the peak load, ε is a constant related to the geometry of the indenter and S is the unloading stiffness at the peak load. S can be determined from the initial unloading slope at P_{max} as follows [31, 32]:

$$S = \frac{dP}{dh} = \beta\frac{2}{\sqrt{\pi}}E_r\sqrt{A_C} \quad (4)$$

where P and h indicate the applied load and penetration depth during nanoindentation, respectively, the term β is a constant related to indenter geometry (β = 1.034 for a Berkovich indenter) [33] and E_r is the reduced elastic modulus defined as:

$$\frac{1}{E_r} = \frac{1-\nu^2}{E} + \frac{1-\nu_i^2}{E_i} \quad (5)$$

here, E_i and ν_i represent the elastic modulus and Poisson's ratio of the indenter, while E and ν are the corresponding values for the specimen [30].

In addition to the nanoindentation tests, dry sliding wear testing was performed at room temperature using a pin-on-disk tribometer testing machine according to the ASTM G99 standard. The cylindrical CP-Ti and Ti-TiB samples (5 mm diameter × 20 mm height) produced by SLM were abraded against a hardened steel disk under a constant load of 40 N with a sliding velocity of 0.54 m/s and a total sliding distance of 250 m. Then, the wear resistance of the SLM-produced samples was evaluated using the weight loss method by measuring the weight of the samples before and after the wear test using an accurate microbalance. SEM was also used to study the worn surfaces of the samples.

3. Results and discussion

Figs. 1 (a-b) show the microstructural characteristics of CP-Ti parts after SLM processing and after casting. It is noteworthy that SLM-produced CP-Ti shows an acicular martensitic (α′) phase structure, whereas the cast-fabricated counterpart indicates a plate-like (α) phase structure similar to those reported in previous works [34, 35]. Moreover, the average width of α′ (~1.06 μm) in the microstructure of the SLM-fabricated CP-Ti is smaller than that of α in the cast CP-Ti sample (~1.88 μm). The martensitic phase and grain refinement observed in SLM-produced CP-Ti can be attributed to a very high cooling rate (10^3 – 10^8 K/s) during SLM [22].

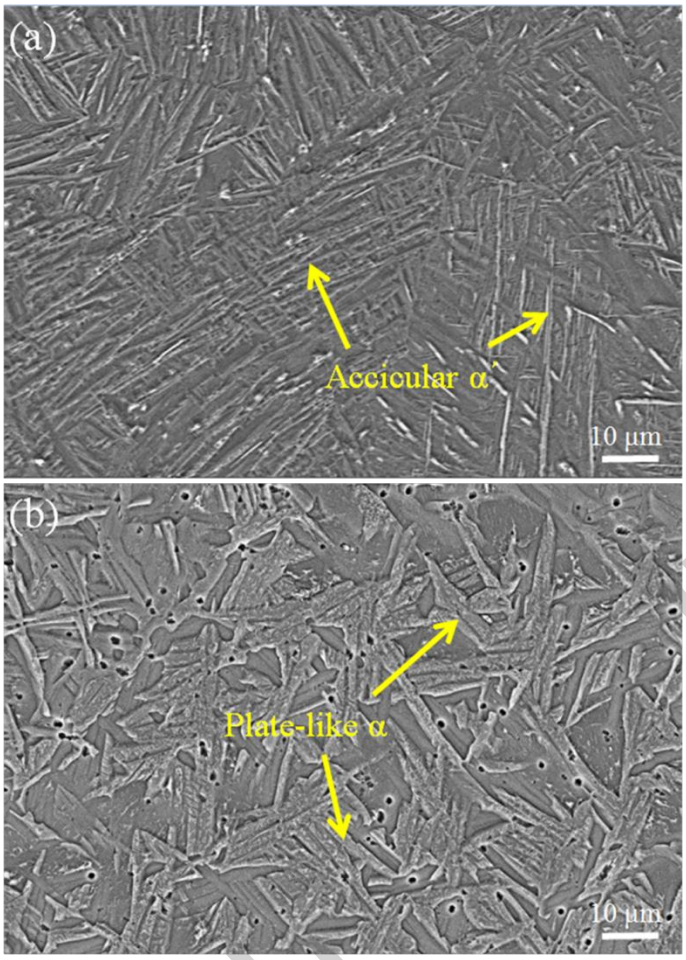

Fig. 1 SEM images of CP-Ti produced by (a) SLM and (b) casting.

SEM and TEM observations of the composite sample indicate the presence of TiB particles with needle-like morphology distributed across the α-Ti matrix (Fig. 2). It has been shown that [36] the formation free-energy of TiB particles by a reaction between Ti and TiB_2 is negative and this reaction is favored when the amount of boron is less than 18.5 wt%. As the boron solubility in titanium is very low (below 0.02wt% at room temperature [37]), during laser melting of the Ti-TiB_2, TiB_2 is transformed into TiB through in-situ chemical reaction between the Ti and TiB_2 [27]. In fact, the reaction between Ti and TiB_2 is exothermic [38] and this reaction may also act as an additional source of heat in the melt pool which supports intermixing of the powders, leading to a fine and random distribution of TiB reinforcements across the Ti matrix similar to

the Ti-TiB composite materials produced by laser engineered net shaping (LENS) [39]. A similar reaction between various types of titanium materials and boron or its compounds has been also observed in other previous works using different technologies [27, 34, 40-42] for the formation of titanium-based composite materials. The reason for the formation of an α-Ti matrix in the Ti-TiB composite material is related to boron's tendency to reduce the martensitic transformation temperatures [43].

In the present work, the diameter and length ranges for needle-like TiB particles are around 30-50 nm and 0.7-1.5 μm, respectively and the average width of the α-Ti grains is 0.75 μm. The titanium grain refinement observed in the Ti-TiB composite compared to that of CP-Ti is mainly related to the rejection of boron during solidification which restricts the growth rate of the primary β-Ti grains [44-46]. According to the Ti-B phase diagram [44], solidification of Ti-TiB occurs in the hypoeutectic zone as the boron content was measured by chemical analysis method (inductively coupled plasma atomic emission spectroscopy) to be around 1.5 wt% for the SLM-processed Ti-TiB material. Accordingly, the TiB phase is formed after the primary β-Ti and it is reasoned that the TiB particles cannot act as nucleation sites for formation of β-Ti, thus grain refinement via inoculation is not expected to occur [44]. The partitioning of boron has also been shown to promote a transformation of the β-grain morphology from a planar (or globular) interface to a dendritic interface. The TiB intermetallics distribute in the interdendritic regions and result in significant refinement of the α-microstructure by reducing the α-colony size. The mechanism for this refinement is proposed to be increased nucleation directly on TiB, on grain boundary impurities and potentially on the prior-β grain boundaries themselves [45]. This mechanism has been shown to be an effective means to refine the α phase structure in titanium fabricated using additive layer manufacturing technologies, even in the case of trace boron additions [47].

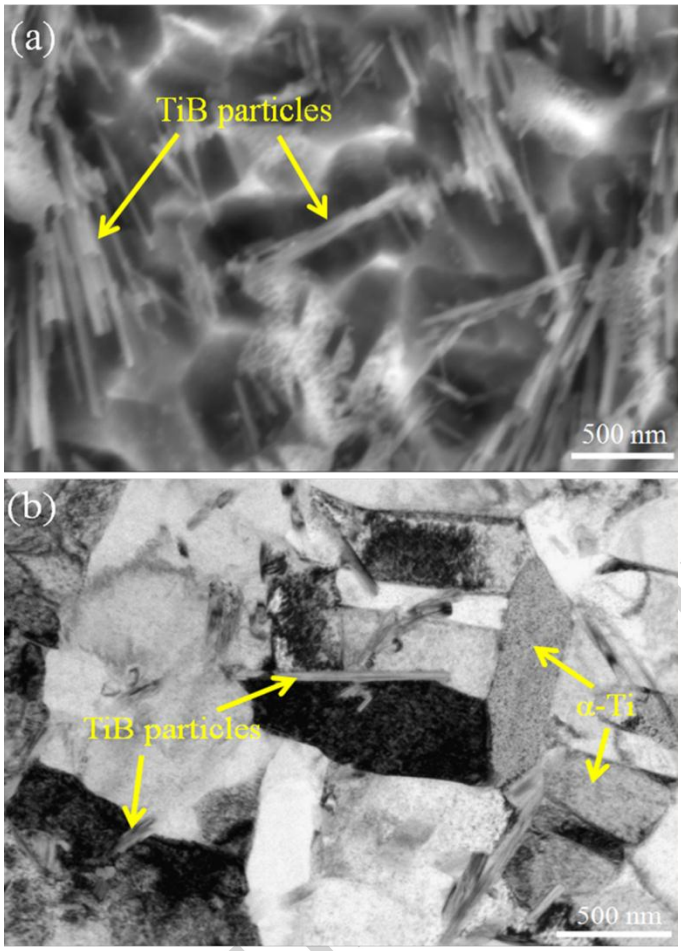

Fig. 2 (a) SEM and (b) bright-field TEM images of Ti-TiB composite materials after SLM processing.

Figs. 3 (a-b) show the nanoindentation load-depth curves for SLM-processed CP-Ti and Ti-TiB materials with increasing loads from 2 mN to 10 mN. Fig. 4 shows an SEM image of the indentations applied on the CP-Ti sample. The curves show three segments: loading, holding at maximum load and unloading. The curves have a smooth shape without evidence of pop-in effects. Larger values of maximum penetration depth, obtained at the end of loading, were observed for CP-Ti for all applied loads, demonstrating that this material possesses lower hardness than Ti-TiB (Figs. 3 (a-b)). Table 1 summarizes the values of H and E_r obtained for the CP-Ti and Ti-TiB composite materials by nanoindentation with different loads. As can be seen, the hardness values for the Ti-TiB composite material are rather high (3.33 - 4.75 GPa) and are

greater than those obtained for CP-Ti (2.39 - 3.64 GPa) mainly due to the hardening effect induced by the TiB particles dispersed throughout the Ti matrix. It has been also reported that hardness is inversely proportional to the material's grain size in accordance with the Hall-Petch relationship [48]. Therefore, the greater hardness values obtained for the Ti-TiB composite can also be related to titanium grain refinement due to boron as described earlier.

According to Table 1, it is also evident that the hardness values decrease with increasing indentation test load. This type of trend can be attributed to indentation size effects (ISE) [49]. In general, the ISE phenomenon involves a reduction in the measured hardness with increasing applied test loads and is associated with differing degrees of dislocation activity around the indents [50]. Thus, this effect makes it difficult to report a hardness value from only one indentation load. Therefore, it is essential to compare the resulting nanoindentation values with those obtained from conventional mechanical testing methods in order to evaluate the optimum nanoindentation load to characterize the hardness of a given material. To this end, the Vickers microhardness values of SLM-fabricated CP-Ti (261 Hv) and Ti-TiB (402 Hv) materials obtained in previous work [27] have been converted to the unit of GPa [51] and are summarized in Table 1.

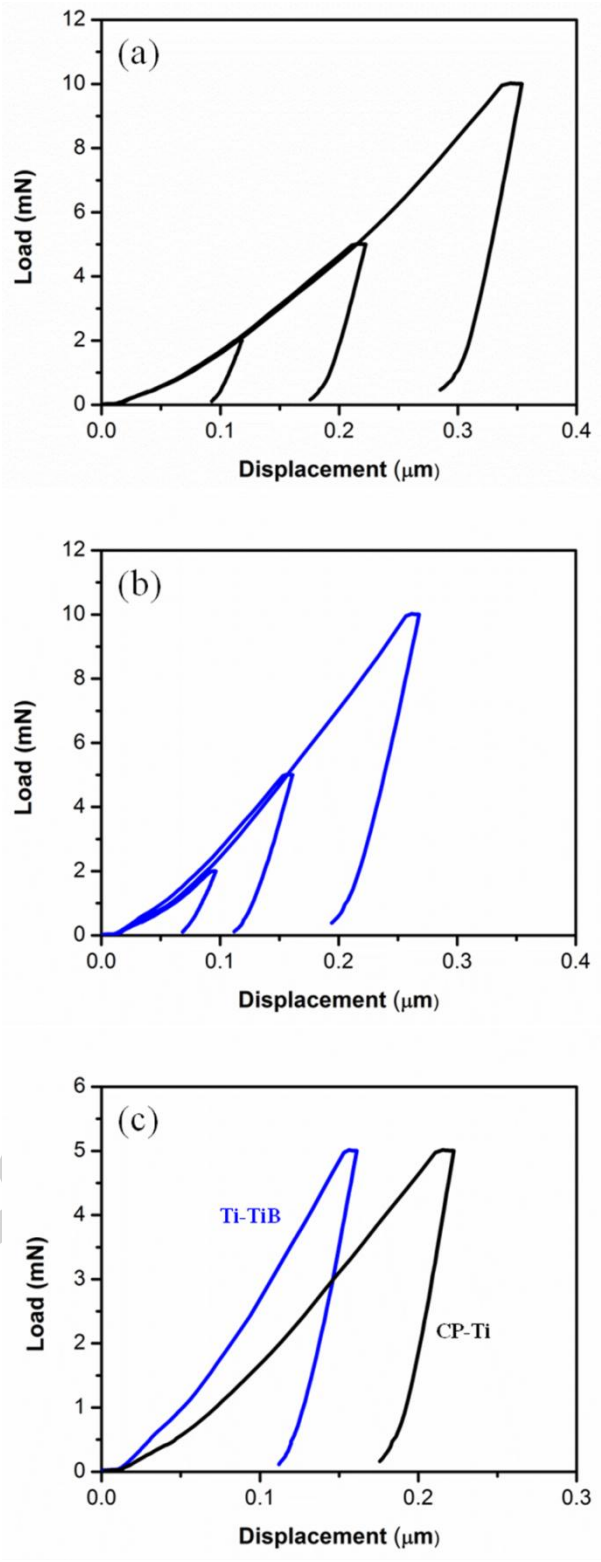

Fig. 3 Nanoindentation load-displacement curves of the SLM-fabricated (a) CP-Ti and (b) Ti-TiB composite materials at loads of 2, 5 and 10 mN; (c) Comparative nanoindentation curves of CP-Ti and Ti-TiB at a load of 5mN.

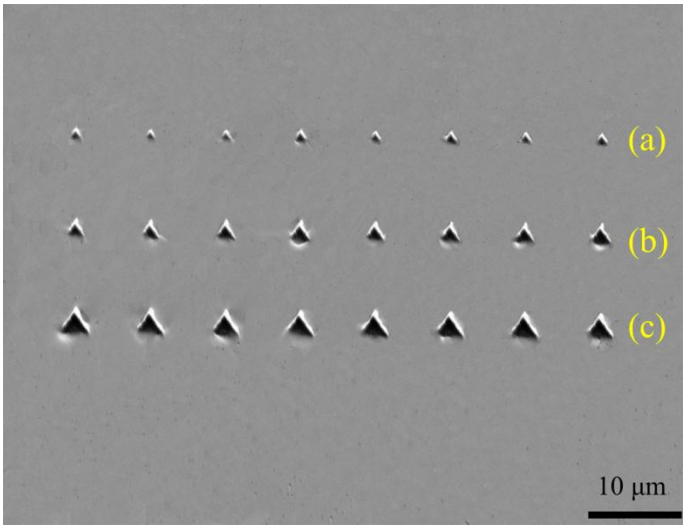

Fig. 4 SEM image of the SLM-fabricated CP-Ti after nanoindentation with different loads of (a) 2 mN, (b) 5 mN and (c) 10 mN.

It is evident that the nanoindentation hardness of CP-Ti (2.95 GPa) and Ti-TiB (4.49 GPa) materials tested with a load of 5 mN is close to those values obtained from the Vickers method (Table 1 and Fig. 3(c)). It is also noted that hardness values obtained with the 5mN load for CP-Ti and Ti-TiB composite materials show good consistency with other published works [52-54], as can be seen in Table 1.

As mentioned, the unloading curves were analyzed using the Oliver-Pharr method to determine the E_r values. As can be seen in Fig. 3 (c), the initial slope of the unloading indentation segment (i.e. the contact stiffness) is higher for Ti-TiB relative to CP-Ti, indicating that Ti-TiB has a higher E_r. Table 1 also lists the values of reduced elastic modulus (E_r) for both CP-Ti and Ti-TiB composite materials. The E_r values for CP-Ti and Ti-TiB composite are in the range of 102 - 134 GPa and 122 – 153 GPa, respectively. Additionally, the Ti-TiB material exhibit higher values of E_r compared to those of CP-Ti which can be related to the stiffening effect induced by the TiB particles.

Table 1 Comparison of mechanical properties of the SLM-fabricated CP-Ti and Ti-TiB materials obtained by nanoindentation and conventional methods. E_r indicates reduced elastic modulus, E is the elastic modulus and H denotes Vickers hardness.

Material	Nanoindentation Load (mN)	E_r (GPa)	E (GPa)	*Nanohardness* (GPa)	H (GPa)	Reference
CP-Ti	2	134	-	3.64	-	This work
	5	116	-	2.95	-	This work
	10	102	-	2.39	-	This work
Ti-TiB	2	153	-	4.75	-	This work
	5	149	-	4.49	-	This work
	10	122	-	3.33	-	This work
CP-Ti	-	-	113	-	2.75	[22, 34]
CP-Ti	-	-	112	-	2.7	[52]
CP-Ti	-	-	119	-	-	[55]
Ti-TiB	-	-	145	-	4.23	[27, 34]
Ti-TiB	-	-	-	-	4.3	[53]
Ti-TiB	-	-	142	-	4.26	[54]

From Table 1, it is evident that variations of the reduced elastic modulus with applied loads are pronounced for both CP-Ti and Ti-TiB materials, similar to the trend observed in nanoindentation hardness values suggesting that elastic modulus of the studied materials is load dependent. Therefore, it is again shown that the reduced elastic modulus cannot be properly characterized by nanoindentation using one load, unless an optimal load value has been determined. As reported in previous work [34], the elastic modulus values obtained from compression testing of the SLM-fabricated CP-Ti and Ti-TiB composite materials are 113 GPa and 145 GPa respectively. The comparison between the elastic modulus values obtained from compression and nanoindentation again indicates that 5 mN is a suitable load for measuring the elastic moduli of SLM-fabricated CP-Ti and Ti-TiB materials using nanoindentation. In addition, the elastic modulus for CP-Ti (116 GPa) obtained using the 5mN load shows good consistency with previous nanoindentation studies of the CP-Ti elastic modulus (119 GPa and 112 GPa [52, 55]). It is also noteworthy that the elastic modulus of the Ti-TiB material obtained using the 5mN load (149 GPa) is close to that

reported for cast-fabricated Ti-TiB material (142 GPa) [54]. Since the same conclusion was also drawn for hardness, it is proposed that 5mN is an optimal load for testing hardness and elastic modulus of the aforementioned materials for consistency with those derived from conventional Vickers hardness and compression tests.

A number of mechanisms are believed to account for the strength increase associated with TiB reinforcements in Ti-TiB composites and the effects of short oriented TiB reinforcement on composite strength and modulus have previously been rationalized using micromechanical models [56]. In the case of the SLM-fabricated Ti-TiB composite, microstructural observations suggest that the orientation of the discontinuous TiB reinforcements is approximately random [27] in which case a simple rule of mixtures approach can be used in order to estimate the stiffness of the composite material. In this case, the modulus of the composite (E_c) is given by:

$$E_c = E_{TiB}V_{TiB} + E_{Ti}V_{Ti} \quad (6)$$

where E_{TiB} is the modulus of the TiB, V_{TiB} is the volume fraction of the TiB, E_{Ti} is the modulus of the titanium matrix and V_{Ti} is the volume fraction of the titanium matrix. Boron reportedly has a very low solubility in titanium below 0.02 wt% at room temperature [37]. Based on the assumption that all boron which is not in solution in titanium reacts to form TiB and given that the relative densities of the Ti and TiB phases are 4.51 gcm^{-3} and 4.54 gcm^{-3} [27], respectively, the estimated volume fraction of the TiB phase, V_{TiB}, is 8.30 vol.%. Then incorporating values of 116 GPa for the modulus of titanium, E_{Ti}, and 480 GPa for the modulus of TiB [57], E_{TiB}, into equation (6) yields 146 GPa for the estimated modulus of the Ti-TiB composite. This is in good agreement with the bulk and nanoindentation derived values and supports the assertion that the needle-like TiB reinforcements are randomly oriented in the Ti matrix.

In addition to the reduced elastic modulus and hardness, nanoindentation can be used to assess the wear resistance of a material [30]. In fact, it is increasingly recognized that the wear

resistance of a material is related to its ability to resist elastic strain to failure at the nanometer scale which is indicated by the ratio of hardness to reduced modulus (H/E_r) [33, 58]. A combination of high hardness and low elastic modulus typically indicates good wear properties [33]. Another parameter, H^3/E_r^2, referred to as yield pressure [33, 59], shows the resistance to plastic deformation. Therefore, this parameter can also be used to evaluate the anti-wear capabilities, since wear caused by gradual removal of a material is reliant on plastic deformation [58]. In the current study, the reduced elastic modulus and the hardness at the testing load of 5mN were used to determine H/E_r and H^3/E_r^2 for both SLM-produced CP-Ti and Ti-TiB materials. The obtained values are around (0.025 and 0.002 GPa for CP-Ti, respectively) and (0.030 and 0.004 GPa for Ti-TiB, respectively) indicating a higher wear resistance for the Ti-TiB composite than the CP-Ti. This concurs with the weight loss of 0.055 g and 0.021 g for CP-Ti and Ti-TiB materials, respectively, determined from conventional wear testing.

Fig. 5 shows typical surface features of worn samples which include ploughing grooves and delamination across the surfaces. It is evident that the worn surface of the SLM-fabricated CP-Ti shows deeper wear scars and more significant delamination than the Ti-TiB material which can be related to its lower hardness relative to Ti-TiB. According to Archard's wear equation [60], the volume of wear is inversely proportional to the hardness of the material under investigation. Therefore, CP-Ti which exhibits lower hardness has undergone higher surface and subsurface plastic deformation which leads to increased delamination and more material removal. This results in increased surface roughness and, consequently, higher abrasion rates of CP-Ti compared to the Ti-TiB material. Enhanced wear properties are an important factor for various industrial applications of titanium based materials, especially in the biomedical area because orthopedic implants are usually subjected to abrasion with surrounding bone and hard tissue. Thus, enhanced wear resistance can reduce the formation of wear particles which can cause

inflammatory reactions, resulting in loosening of the implant and the subsequent need for revision surgery [1, 61].

Finally, it is concluded that the nanoindentation load can be appropriately adjusted to measure mechanical properties including hardness and elastic modulus to give good consistency to those values obtained from conventional mechanical tests. It was also shown that nanoindentation can be used to evaluate the wear resistance of the SLM-fabricated CP-Ti and Ti-TiB materials. This is very important for the production of SLM titanium parts of small sizes, unusual geometries or for those that may require regular inspection and testing during their operational lifetime.

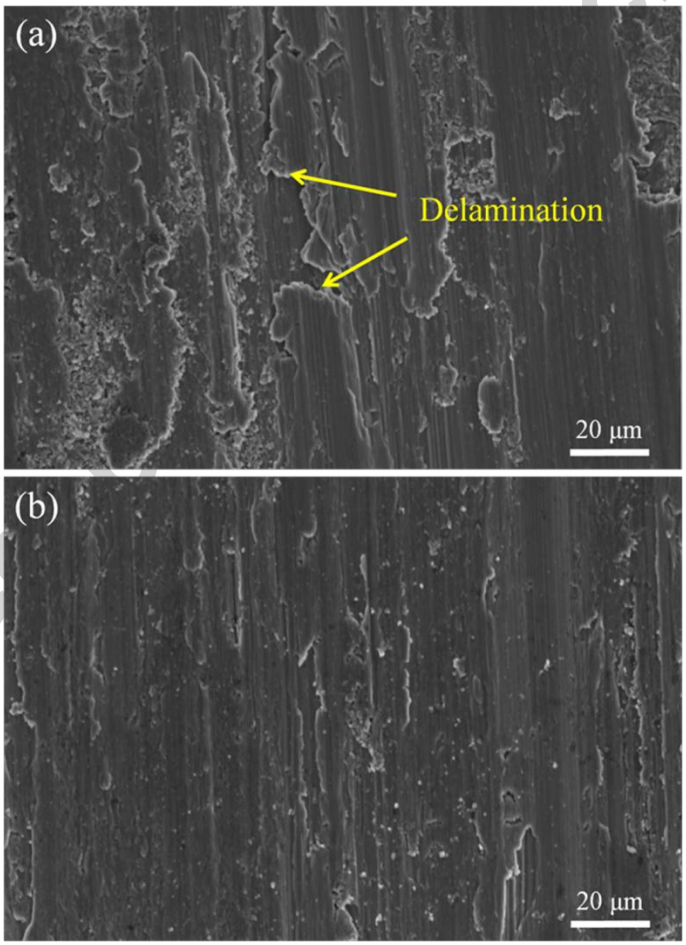

Fig. 5 SEM images of worn surfaces after wear testing of (a) CP-Ti and (b) Ti-TiB composite materials produced by SLM.

4. Conclusions

In this study, CP-Ti and Ti-TiB composite materials were processed by selective laser melting (SLM). CP-Ti had an acicular martensitic (α′) microstructure due to the high cooling rates present during SLM. In contrast, the Ti-TiB material showed a fine distribution of TiB particles, formed by in-situ chemical reaction between Ti and TiB_2 powders, dispersed within an α-Ti matrix. Hardness and reduced elastic modulus measured by nanoindentation were higher for Ti-TiB composite than those of CP-Ti due to hardening and stiffening effects induced by the TiB particles as well as titanium grain refinement due to boron. It was also observed that CP-Ti possesses lower wear resistance compared to Ti-TiB composite likely due to its lower hardness and lowered resistance to elastic strain to failure. Although nanoindentation testing showed a dependency for both hardness and elastic modulus on the applied load, it demonstrated that the values obtained from a 5 mN load had high consistency with those from conventional mechanical tests. It is proposed that 5 mN is an optimal load for measurement of elastic modulus and hardness properties of the titanium materials studied in this work.

Acknowledgment

This research was supported from the European Commission (BioTiNet-ITN G.A. 264635).

References

[1] M. Geetha, A. Singh, R. Asokamani, A. Gogia, Ti based biomaterials, the ultimate choice for orthopaedic implants–a review, Prog Mater Sci, 54 (2009) 397-425.

[2] D. Banerjee, J. Williams, Perspectives on titanium science and technology, Acta Mater, 61 (2013) 844-879.

[3] I.V. Okulov, H. Wendrock, A.S. Volegov, H. Attar, U. Kühn, W. Skrotzki, J. Eckert, High strength beta titanium alloys: New design approach, Mater Sci Eng A, 628 (2015) 297-302.

[4] I. Okulov, U. Kühn, T. Marr, J. Freudenberger, I. Soldatov, L. Schultz, C.-G. Oertel, W. Skrotzki, J. Eckert, Microstructure and mechanical properties of new composite structured Ti–V–Al–Cu–Ni alloys for spring applications, Mater Sci Eng A, 603 (2014) 76-83.

[5] S. Ehtemam-Haghighi, K. Prashanth, H. Attar, A.K. Chaubey, G. Cao, L. Zhang, Evaluation of mechanical and wear properties of Ti-xNb-7Fe alloys designed for biomedical applications, Mater Des, 111 (2016) 592-599.

[6] Y. Zhang, D. Kent, G. Wang, D. St John, M. Dargusch, An investigation of the mechanical behaviour of fine tubes fabricated from a Ti–25Nb–3Mo–3Zr–2Sn alloy, Mater Des, 85 (2015) 256-265.

[7] M.A.-H. Gepreel, M. Niinomi, Biocompatibility of Ti-alloys for long-term implantation, J Mech Behav Biomed Mater 20 (2013) 407-415.

[8] S.E. Haghighi, H. Lu, G. Jian, G. Cao, D. Habibi, L. Zhang, Effect of α ″martensite on the microstructure and mechanical properties of beta-type Ti–Fe–Ta alloys, Mater Des, 76 (2015) 47-54.

[9] I. Okulov, A. Volegov, H. Attar, M. Bönisch, S. Ehtemam-Haghighi, M. Calin, J. Eckert, Composition optimization of low modulus and high-strength TiNb-based alloys for biomedical applications, J Mech Behav Biomed Mater 65 (2017) 866-871.

[10] I. Okulov, S. Pauly, U. Kühn, P. Gargarella, T. Marr, J. Freudenberger, L. Schultz, J. Scharnweber, C.-G. Oertel, W. Skrotzki, Effect of microstructure on the mechanical properties of as-cast Ti–Nb–Al–Cu–Ni alloys for biomedical application, Mater Sci Eng C, 33 (2013) 4795-4801.

[11] K. Morsi, V. Patel, Processing and properties of titanium–titanium boride (TiBw) matrix composites—a review, J Mater Sci 42 (2007) 2037-2047.

[12] B.-J. Choi, I.-Y. Kim, Y.-Z. Lee, Y.-J. Kim, Microstructure and friction/wear behavior of (TiB+ TiC) particulate-reinforced titanium matrix composites, Wear, 318 (2014) 68-77.

[13] N. Read, W. Wang, K. Essa, M.M. Attallah, Selective laser melting of AlSi10Mg alloy: Process optimisation and mechanical properties development, Mater Des, 65 (2015) 417-424.

[14] Z. Wang, K. Guan, M. Gao, X. Li, X. Chen, X. Zeng, The microstructure and mechanical properties of deposited-IN718 by selective laser melting, J Alloys Compd, 513 (2012) 518-523.

[15] C. Yan, L. Hao, A. Hussein, P. Young, D. Raymont, Advanced lightweight 316L stainless steel cellular lattice structures fabricated via selective laser melting, Mater Des, 55 (2014) 533-541.

[16] S. Scudino, C. Unterdörfer, K. Prashanth, H. Attar, N. Ellendt, V. Uhlenwinkel, J. Eckert, Additive manufacturing of Cu–10Sn bronze, Mater Lett, 156 (2015) 202-204.

[17] L. Yan, Y. Yuan, L. Ouyang, H. Li, A. Mirzasadeghi, L. Li, Improved mechanical properties of the new Ti-15Ta-xZr alloys fabricated by selective laser melting for biomedical application, J Alloys Compd, 688 (2016) 156-162.

[18] I. Yadroitsev, P. Krakhmalev, I. Yadroitsava, Selective laser melting of Ti6Al4V alloy for biomedical applications: Temperature monitoring and microstructural evolution, J Alloys Compd, 583 (2014) 404-409.

[19] D. Gu, Y.-C. Hagedorn, W. Meiners, G. Meng, R.J.S. Batista, K. Wissenbach, R. Poprawe, Densification behavior, microstructure evolution, and wear performance of selective laser melting processed commercially pure titanium, Acta Mater, 60 (2012) 3849-3860.

[20] L. Thijs, F. Verhaeghe, T. Craeghs, J. Van Humbeeck, J.-P. Kruth, A study of the microstructural evolution during selective laser melting of Ti–6Al–4V, Acta Mater, 58 (2010) 3303-3312.

[21] C. Yan, L. Hao, A. Hussein, D. Raymont, Evaluations of cellular lattice structures manufactured using selective laser melting, Int J Mach Tool Manufact, 62 (2012) 32-38.

[22] H. Attar, M. Calin, L. Zhang, S. Scudino, J. Eckert, Manufacture by selective laser melting and mechanical behavior of commercially pure titanium, Mater Sci Eng A, 593 (2014) 170-177.

[23] A. Fukuda, M. Takemoto, T. Saito, S. Fujibayashi, M. Neo, D.K. Pattanayak, T. Matsushita, K. Sasaki, N. Nishida, T. Kokubo, Osteoinduction of porous Ti implants with a channel structure fabricated by selective laser melting, Acta Biomater, 7 (2011) 2327-2336.

[24] C. Ng, M. Savalani, M. Lau, H. Man, Microstructure and mechanical properties of selective laser melted magnesium, Appl Surf Sci 257 (2011) 7447-7454.

[25] D. Cáceres, C. Munuera, C. Ocal, J.A. Jiménez, A. Gutiérrez, M. López, Nanomechanical properties of surface-modified titanium alloys for biomedical applications, Acta Biomater, 4 (2008) 1545-1552.

[26] D. Gu, Y.-C. Hagedorn, W. Meiners, K. Wissenbach, R. Poprawe, Nanocrystalline TiC reinforced Ti matrix bulk-form nanocomposites by selective laser melting (SLM): Densification, growth mechanism and wear behavior, Compos Sci Technol, 71 (2011) 1612-1620.

[27] H. Attar, M. Bönisch, M. Calin, L.-C. Zhang, S. Scudino, J. Eckert, Selective laser melting of in situ titanium–titanium boride composites: processing, microstructure and mechanical properties, Acta Mater, 76 (2014) 13-22.

[28] W.C. Oliver, G.M. Pharr, An improved technique for determining hardness and elastic modulus using load and displacement sensing indentation experiments, J Mater Res, 7 (1992) 1564-1583.

[29] S.S. Singh, C. Schwartzstein, J.J. Williams, X. Xiao, F. De Carlo, N. Chawla, 3D microstructural characterization and mechanical properties of constituent particles in Al 7075 alloys using X-ray synchrotron tomography and nanoindentation, J Alloys Compd, 602 (2014) 163-174.

[30] M. Masanta, S. Shariff, A.R. Choudhury, Evaluation of modulus of elasticity, nano-hardness and fracture toughness of TiB 2–TiC–Al 2 O 3 composite coating developed by SHS and laser cladding, Mater Sci Eng A, 528 (2011) 5327-5335.

[31] A. Ozmetin, O. Sahin, E. Ongun, M. Kuru, Mechanical characterization of MgB 2 thin films using nanoindentation technique, J Alloys Compd, 619 (2015) 262-266.

[32] B. Medeiros, M. Medeiros, J. Fornell, J. Sort, M. Baró, A. Jorge, Nanoindentation response of Cu–Ti based metallic glasses: Comparison between as-cast, relaxed and devitrified states, J Non-Cryst Solids, 425 (2015) 103-109.

[33] A. Hynowska, E. Pellicer, J. Fornell, S. González, N. Van Steenberge, S. Suriñach, A. Gebert, M. Calin, J. Eckert, M.D. Baró, Nanostructured β-phase Ti–31.0 Fe–9.0 Sn and sub-μm structured Ti–39.3 Nb–13.3 Zr–10.7 Ta alloys for biomedical applications: Microstructure benefits on the mechanical and corrosion performances, Mater Sci Eng C, 32 (2012) 2418-2425.

[34] H. Attar, L. Löber, A. Funk, M. Calin, L. Zhang, K. Prashanth, S. Scudino, Y. Zhang, J. Eckert, Mechanical behavior of porous commercially pure Ti and Ti–TiB composite materials manufactured by selective laser melting, Mater Sci Eng A, 625 (2015) 350-356.

[35] H. Attar, K. Prashanth, A. Chaubey, M. Calin, L. Zhang, S. Scudino, J. Eckert, Comparison of wear properties of commercially pure titanium prepared by selective laser melting and casting processes, Mater Lett, 142 (2015) 38-41.

[36] K. Panda, K.R. Chandran, Synthesis of ductile titanium-titanium boride (Ti-TiB) composites with a beta-titanium matrix: The nature of TiB formation and composite properties, Metall Mater Trans A, 34 (2003) 1371-1385.

[37] J. Luan, Z. Jiao, G. Chen, C. Liu, Improved ductility and oxidation resistance of cast Ti–6Al–4V alloys by microalloying, J Alloys Compd, 602 (2014) 235-240.

[38] D. Galvan, V. Ocelik, Y. Pei, B. Kooi, J.T.M. De Hosson, E. Ramous, Microstructure and properties of TiB/Ti-6Al-4V coatings produced with laser treatments, J Mater Eng Perform 13 (2004) 406-412.

[39] R. Banerjee, P.C. Collins, H.L. Fraser, Laser deposition of in situ Ti–TiB composites, Adv Eng Mater, 4 (2002) 847-851.

[40] S. Gorsse, D. Miracle, Mechanical properties of Ti-6Al-4V/TiB composites with randomly oriented and aligned TiB reinforcements, Acta Mater, 51 (2003) 2427-2442.

[41] V. Imayev, R. Gaisin, R. Imayev, Effect of boron additions and processing on microstructure and mechanical properties of a titanium alloy Ti–6.5 Al–3.3 Mo–0.3 Si, Mater Sci Eng A, 641 (2015) 71-83.

[42] S. Gorsse, J. Chaminade, Y. Le Petitcorps, In situ preparation of titanium base composites reinforced by TiB single crystals using a powder metallurgy technique, Compos Part A Appl S, 29 (1998) 1229-1234.

[43] Y. Horiuchi, T. Inamura, H.Y. Kim, K. Wakashima, S. Miyazaki, H. Hosoda, Effect of boron concentration on martensitic transformation temperatures, stress for inducing martensite and slip stress of Ti-24 mol% Nb-3 mol% Al superelastic alloy, Mater Trans, 48 (2007) 407-413.

[44] S. Tamirisakandala, R. Bhat, J. Tiley, D. Miracle, Grain refinement of cast titanium alloys via trace boron addition, Scripta Mater, 53 (2005) 1421-1426.

[45] M. Bermingham, S. McDonald, K. Nogita, D.S. John, M. Dargusch, Effects of boron on microstructure in cast titanium alloys, Scripta Mater, 59 (2008) 538-541.

[46] I. Okulov, M. Sarmanova, A. Volegov, A. Okulov, U. Kühn, W. Skrotzki, J. Eckert, Effect of boron on microstructure and mechanical properties of multicomponent titanium alloys, Mater Lett, 158 (2015) 111-114.

[47] M. Bermingham, D. Kent, H. Zhan, D. StJohn, M. Dargusch, Controlling the microstructure and properties of wire arc additive manufactured Ti–6Al–4V with trace boron additions, Acta Mater, 91 (2015) 289-303.

[48] A. Sergueeva, V. Stolyarov, R. Valiev, A. Mukherjee, Advanced mechanical properties of pure titanium with ultrafine grained structure, Scripta Mater, 45 (2001) 747-752.

[49] Z. Peng, J. Gong, H. Miao, On the description of indentation size effect in hardness testing for ceramics: Analysis of the nanoindentation data, J Eur Cera Soc 24 (2004) 2193-2201.

[50] A. Elmustafa, D. Stone, Nanoindentation and the indentation size effect: Kinetics of deformation and strain gradient plasticity, J Mech Phys Solids, 51 (2003) 357-381.

[51] Y. Sun, J. Liang, Z.-H. Xu, G. Wang, X. Li, Nanoindentation for measuring individual phase mechanical properties of lead free solder alloy, J Mater Sci Mater Electron, 19 (2008) 514-521.

[52] S. Abdi, M.S. Khoshkhoo, O. Shuleshova, M. Bönisch, M. Calin, L. Schultz, J. Eckert, M. Baró, J. Sort, A. Gebert, Effect of Nb addition on microstructure evolution and nanomechanical properties of a glass-forming Ti–Zr–Si alloy, Intermetallics, 46 (2014) 156-163.

[53] S. Wei, Z.-H. Zhang, F.-C. Wang, X.-B. Shen, H.-N. Cai, S.-K. Lee, L. Wang, Effect of Ti content and sintering temperature on the microstructures and mechanical properties of TiB reinforced titanium composites synthesized by SPS process, Mater Sci Eng A, 560 (2013) 249-255.

[54] H. Attar, M. Bönisch, M. Calin, L.C. Zhang, K. Zhuravleva, A. Funk, S. Scudino, C. Yang, J. Eckert, Comparative study of microstructures and mechanical properties of in situ Ti–TiB composites produced by selective laser melting, powder metallurgy, and casting technologies, J Mater Res, 29 (2014) 1941-1950.

[55] P. Majumdar, S. Singh, M. Chakraborty, Elastic modulus of biomedical titanium alloys by nano-indentation and ultrasonic techniques—A comparative study, Mater Sci Eng A, 489 (2008) 419-425.

[56] T. Srivatsan, W. Soboyejo, R. Lederich, Tensile deformation and fracture behaviour of a titanium-alloy metal-matrix composite, Compos Part A Appl S, 28 (1997) 365-376.

[57] W. Soboyejo, R. Lederich, S. Sastry, Mechanical behavior of damage tolerant TiB whisker-reinforced in situ titanium matrix composites, Acta Metall Mater 42 (1994) 2579-2591.

[58] J. Xu, G. dong Wang, X. Lu, L. Liu, P. Munroe, Z.-H. Xie, Mechanical and corrosion-resistant properties of Ti–Nb–Si–N nanocomposite films prepared by a double glow discharge plasma technique, Ceram Int, 40 (2014) 8621-8630.

[59] J. Fornell, N. Van Steenberge, A. Varea, E. Rossinyol, E. Pellicer, S. Suriñach, M. Baró, J. Sort, Enhanced mechanical properties and in vitro corrosion behavior of amorphous and devitrified Ti 40 Zr 10 Cu 38 Pd 12 metallic glass, J Mech Behav Biomed Mater 4(2011) 1709-1717.

[60] Q. Wang, P.-Z. Zhang, D.-B. Wei, X.-H. Chen, R.-N. Wang, H.-Y. Wang, K.-T. Feng, Microstructure and sliding wear behavior of pure titanium surface modified by double-glow plasma surface alloying with Nb, Mater Des, 52 (2013) 265-273.

[61] S. Ehtemam-Haghighi, G. Cao, L.-C. Zhang, Nanoindentation study of mechanical properties of Ti based alloys with Fe and Ta additions, J Alloys Compd, 692 (2017) 892-897.